PHYSICAL REVIEW A **82**, 061803(R) (2010)

Tailoring the filamentation of intense femtosecond laser pulses with periodic lattices

P. Panagiotopoulos,[1] N. K. Efremidis,[2] D. G. Papazoglou,[1,3] A. Couairon,[4] and S. Tzortzakis[1,*]

[1]*Institute of Electronic Structure and Laser, Foundation for Research and Technology Hellas, P.O. Box 1527, GR-71110 Heraklion, Greece*

[2]*Department of Applied Mathematics, University of Crete, P.O. Box 2208, GR-71003 Heraklion, Greece*

[3]*Department of Materials Science and Technology, University of Crete, P.O. Box 2208, GR-71003 Heraklion, Greece*

[4]*Centre de Physique Théorique, Centre National de la Recherche Scientifique, Ecole Polytechnique, F-91128 Palaiseau, France*

(Received 16 September 2009; published 23 December 2010)

We show numerically that by using periodic lattices the filamentation of intense femtosecond laser pulses, otherwise a result of competing nonlinear effects, can be well controlled with respect to its properties. The diffraction induced by the lattice provides a regularizing mechanism to the nonlinear self-action effects involved in filamentation. We demonstrate a new propagation regime of intense lattice solitons bridging the field of spatial solitons with that of femtosecond laser filamentation. The effective filamentation control is expected to have an important impact on numerous applications.

DOI: 10.1103/PhysRevA.82.061803 PACS number(s): 42.25.Bs, 05.45.Yv, 42.65.Jx, 42.65.Re

Femtosecond laser filamentation in transparent media has grown into one of the most active fields of laser physics in recent years [1]. Filaments appear for input powers close to or above a critical value P_{cr} and are the result of a competition involving linear and highly nonlinear effects, such as the optical Kerr effect, defocusing due to plasma created by optical field ionization, nonlinear losses, and dispersion [1]. Their unique attributes have led to numerous propositions and demonstrations of applications, such as single-cycle pulse generation for attosecond drivers [2,3], electric discharge triggering and guiding [4], remote sensing [5], intense tetrahertz generation [6–8], and many others [1]. For many of these applications, however, the possible use of filaments as tunable intense light channels is still an open question.

Filamentation tailoring denotes the selective optimization of specific filament attributes. Its importance is fundamental in view of the numerous applications of filaments that are promising but have remained compromised up to now by poor control over the filamentation process. For instance, it has recently been shown that the tetrahertz emission from two-color filaments strongly depends on the uniformity of the plasma string and its length [8]. In another example one could consider the use of long filaments at intensities just below ionization for generating higher harmonics and attosecond pulses.

However, as filamentation results from the competition between self-action effects, its attributes are not easily controllable, and control is further hindered by the high intensities in filaments (exceeding 10^{13} W/cm^2 in air) that exclude optical elements from being introduced in their path. Thus, the majority of efforts, to date, were limited to the control of the spatial and temporal characteristics of the initial laser pulses [1]. Examples of these approaches include the use of amplitude and phase masks or the introduction of aberrations on the initial beam wave front [9,10]. More recently, impulsive alignment of molecular gases has been shown to also strongly affect the propagation of laser pulses [11].

To find more efficient ways to control filamentation, one must return to the principles of nonlinear propagation. The propagation of intense pulses under fairly constant intensity and beam waist has also been observed in solitons, where the intensities are much lower than those observed in filaments. In this case, self-focusing induced by the optical Kerr effect is balanced by diffraction or other linear propagation phenomena. Since the intensity never reaches values where multiphoton absorption is important, these pulses propagate practically without losses. However, it is known that in two spatial dimensions the soliton solutions supported by the nonlinear Schrödinger equation are unstable [12,13], leading to diffraction or wave collapse of the initial beam. Nevertheless, it was shown that in the presence of a periodic waveguide lattice, light has the tendency to be localized in the high-index areas, leading to the formation of discrete solitons [14,15]. Interestingly, in a two-dimensional setting, such soliton solutions can be stabilized by the presence of a periodic lattice [16–19]. Experimentally, two-dimensional optical lattice solitons were observed [20] using an optical induction technique [21]. It was already demonstrated that the attributes of solitons can be tailored by using discrete waveguide arrays (see [22] and references therein). In the presence of a periodic potential, self-focusing balances the linear diffraction induced by the waveguide array. Furthermore, the soliton attributes, such as the peak intensity and width, are controlled by the waveguide array parameters and the total input power.

In this Rapid Communication, inspired by the waveguide arrays and optically induced lattices used to control the attributes of solitons, we investigate the use of lattices to control the features of intense femtosecond laser filaments. In this way, we demonstrate a propagation regime of intense lattice solitons bridging the field of spatial solitons with that of filamentation. By tuning the parameters of the lattice, we can tailor the filaments' uniformity, peak intensity, plasma density, beam width, and total length. This tunability is not the result of a linear guiding effect but of an enforced balance between the nonlinear propagation effects and the linear diffraction induced by the lattice.

To start with, we consider a discrete waveguide array structure, similar to that used in [18] to control the attributes of solitons. A proper choice of the array parameters allows for a control of the full width at half maximum and the peak

*stzortz@iesl.forth.gr

intensity of a propagating soliton. Application of this idea to the dynamic propagation of optical pulses during filamentation in gases, without introducing optical materials in their paths, can be realized by using, for instance, plasma photonic lattices that can survive high intensities. Plasma is an ideal candidate for generating a waveguide array structure by interference of intense light beams [23,24] since it withstands damage, in contrast to classical optical elements, while the refractive index of the medium can be easily perturbed with changes as large as $\Delta n \sim 10^{-3}$. Another possibility is to use positive or negative Δn lattices, exploiting the molecular alignment of air molecules (or other gases) [11]. In the latter case the laser intensities needed are lower than the ones needed for ionization, and one can use pulse trains to further enhance the alignment [25] and, consequently, the strength of the lattice.

The numerical model [1] that we use here resolves a nonlinear envelope equation:

$$\frac{\partial E}{\partial z} = \frac{i}{2k_o} T^{-1} \Delta_\perp E - i \frac{k''}{2} \frac{\partial^2 E}{\partial t^2} + N(E^2, \rho) E + i\, k_o T^{-1} \Delta n(x,y) E, \quad (1)$$

which describes the evolution of the slowly varying envelope $E(x,y,z,t)$ of the electric field E of a laser pulse that propagates in the z direction in a transparent Kerr medium. Details on this widely used numerical model can be found in the supplementary material [26]. Before moving to the filamentation regime we confirmed the existence of soliton solutions for a lattice consisting of an array of equally spaced negative Δn rods using a simplified form of Eq. (1), keeping only the diffraction, the Kerr nonlinearity, and the linear potential terms. In this type of lattice, light has the tendency to become localized in the high index areas between the low-index leaky waveguides. Although the Δn maxima are not isolated, this lattice supports stable lattice solitons exhibiting both lower and upper power thresholds. A detailed discussion on these soliton solutions can be found in [26].

We are now interested in the transition from lattice solitons to the regime of single filamentation with power close to $P_{\rm cr}$. We therefore consider the cylindrically symmetric version of Eq. (1) which describes well the single filamentation regime and a cylindrically symmetric waveguide array structure for which stable lattice solitons exist, as in the case of square lattices [26]. The isolated negative index plasma strings are thus transformed into plasma cylinders and the structure now resembles a multilayered waveguide. The refractive index of this structure reads

$$n_{\rm cyl}(x,y,z) = n_o + \Delta n_o \sum_{m=0} f\left[\sqrt{x^2+y^2} - \left(m+\frac{1}{2}\right)\Lambda\right], \quad (2)$$

where $f(r)$is the function describing a generic refractive index distribution, in our case a super-Gaussian of order p, $f(r) = \exp[-(r/w)^{2p}]$; w is the typical width of the distribution $f(r)$ and $p = 8$; Λ is the period of the structures; n_o is the bulk refractive index; and Δn_o is the refractive index modulation amplitude. For the simulations that will be shown here, unless stated otherwise, $w = 100\ \mu$m, $\Lambda = 350\ \mu$m, and $\Delta n_o = -3.3 \times 10^{-7}$, corresponding to electron densities of $\rho_{\rm plasma} \cong 1.14 \times 10^{15}{\rm cm}^{-3}$. The input laser pulse is 35 fs long, with a Gaussian spatiotemporal profile, a central wavelength at 800 nm, and a beam waist of 500 μm ($1/e^2$ radius), with no initial wave-front curvature. Simulations were performed for propagation in air at atmospheric pressure, where the input power is either $10^{-6} P_{\rm cr}$ for the linear regime or 1.25 $P_{\rm cr}$ for the nonlinear regime.

Figure 1 depicts simulation results that show the effect of the lattice on the propagation of pulses in both the linear and nonlinear regimes. Figure 1(a) shows the propagation of the pulse in the linear regime ($10^{-6} P_{\rm cr}$) without the presence of the lattice, which corresponds to diffraction of the beam over 3 m of propagation. As the power is increased to 1.25 $P_{\rm cr}$ the beam self-focuses and reshapes into a typical filament in air, which extends from 125 to 150 cm, as shown in Fig. 1(b). In this case, the peak intensity in the nonlinear focus reaches 3×10^{13} W/cm^2, while the beam waist shrinks down to $\sim$100 μm. At this intensity, multiphoton ionization is not negligible, and the plasma density reaches 10^{16} cm^{-3}. Figures 1(c) and 1(d) show the effect of the lattice on the propagation of the pulse. In the linear regime [Fig. 1(c)], the beam is coupled in the lattice, but the energy gradually spreads out during propagation as a result of diffraction. When the power is increased, the behavior is strikingly different. As shown in Fig. 1(d), a quasistationary soliton-like filament is formed with nearly constant intensity of 5×10^{12} W/cm^2 over 1.8 m of propagation. The peak intensity is about 1 order of magnitude lower than that obtained in the typical filament shown in Fig. 1(b), i.e., not significant enough to generate, through multiphoton ionization, a plasma that could affect propagation. This result clearly demonstrates filamentation tailoring while the balance of the nonlinear propagation effects of the high-power beam with the linear propagation effects induced by the lattice reveals a new regime bridging solitonic and filamentary propagation. This propagation regime is not the result of a linear guiding effect. As shown in Fig. 1(c), where only linear effects are present, the coupling between the concentric waveguide structures leads to the spreading

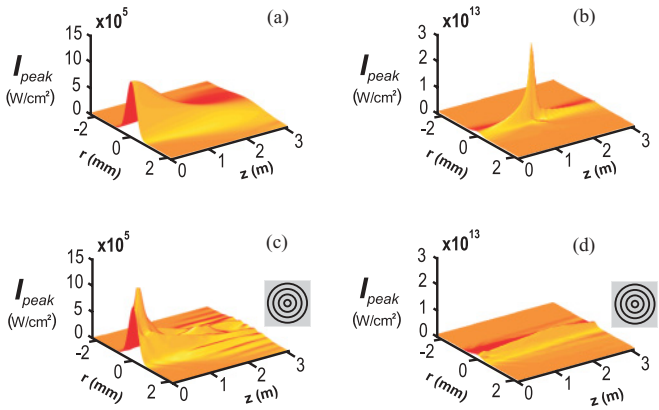

FIG. 1. (Color online) Comparison of peak intensities $I_{\rm peak}$ (r,z) for propagation (a,b) in air and (c,d) in a cylindrical lattice. The left column shows the linear propagation regime $P_{\rm in} = 10^{-6} P_{\rm cr}$, and the right column shows the nonlinear propagation and filamentation regime $P_{\rm in} = 1.25 P_{\rm cr}$. Lattice parameters are $\Lambda = 350\ \mu$m, $w = 100\ \mu$m, and $\Delta n_o = -3.3 \times 10^{-7}$. Insets are graphic representations of the cylindrical lattice, where black represents lower refractive index.

of the energy toward the outer waveguides. On the other hand, practically all the energy is maintained in the central waveguide when the input intensity is high; thus, the nonlinear propagation effects balance the linear diffraction properties of the lattice. In addition, the results of simulations made with a lattice comprising only the central plasma ring are close to the case without lattice and significantly differ from the propagation in the full lattice.

The ability of the waveguide structure to affect filamentation properties is clearly visualized in Fig. 2, which shows the evolution of the filament width as a function of the propagation distance. Without lattice [Fig. 2(a)], the filament width remains fairly constant, around 100 μm, for about 25 cm. Fig. 2(b) depicts the width of the filament tailored by the lattice. The effect of the waveguide structure on the beam waist of the propagating pulse is striking. The lattice leads to an almost-constant beam waist of $\sim$270 μm for a propagation distance of 180 cm. In this case, the beam width actually depends on the lattice period, allowing control over its size and, consequently, its peak intensity.

A systematic study of the effect of lattice parameters (period and modulation) on the propagation of the filament is shown in Figs. 2(c) and 2(d). Figure 2(c) depicts the peak intensity as a function of the propagation distance for various depths Δn_o of the effective refractive index modulation for a constant period of $\Lambda = 350$ μm. The modulation depth Δn_o is varied from 0 (curve i), corresponding to the absence of lattice, to -5.0×10^{-7} (curve v). As the modulation becomes deeper the peak intensity drops, and its distribution is widened and shifted toward longer propagation distances. Furthermore, these curves show that the balance between nonlinear effects and diffraction by the lattice is quite sensitive to the modulation depth Δn_o. Curve iv in Fig. 2(c), with $\Delta n_o = -3.3 \times 10^{-7}$, presents the optimum value for this balance. For weaker modulation depths [curves i, ii, and iii in Fig. 2(c)], the peak intensity is still high, and nonlinear effects (mainly the optical Kerr effect) dominate. By further strengthening the modulation amplitude [curve v in Fig. 2(c)], the peak intensity monotonically decreases due to the prevailing linear effect of the waveguide structure over nonlinear effects.

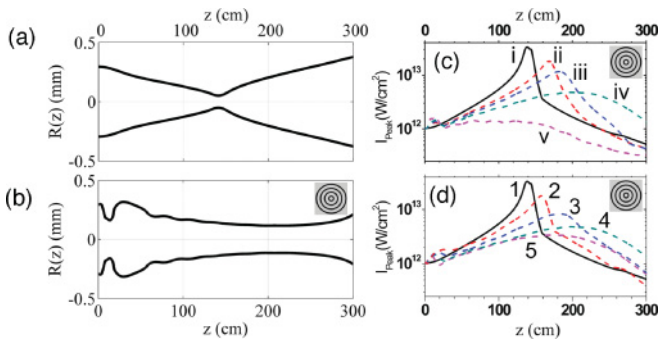

FIG. 2. (Color online) Beam width as a function of the propagation distance z (a) without lattice and (b) with lattice. Peak intensity I_{peak} as a function of the propagation distance z for (c) lattice strengths Δn_o of 0 (curve i), -2×10^{-7} (curve ii), -2.5×10^{-7} (curve iii), -3.3×10^{-7} (curve iv), and -5.0×10^{-7} (curve v) and (d) lattice periodicities Λ of ∞ (curve 1), 450 μm (curve 2), 400 μm (curve 3), 350 μm (curve 4), and 300 μm (curve 5). Insets are graphic representations of the cylindrical lattice, where black represents lower refractive index.

Another important parameter of the lattice that affects the propagation attributes is its period Λ. Figure 2(d) depicts the peak intensity as a function of the propagation distance for various lattice periods for a constant modulation depth $\Delta n_o = -3.3 \times 10^{-7}$. The period Λ is varied from infinity (curve [1]), corresponding to the absence of lattice, down to 300 μm (curve [5]). The behavior is similar to that obtained for a variation of the modulation depth. As the lattice period gets smaller, the peak intensity drops, and its distribution is widened and shifted toward longer propagation distances. As shown by these curves the regime where nonlinear propagation effects and the linear contribution of the lattice are balanced is also sensitive to the period Λ. Curve 4 in Fig. 2(d), for which $\Lambda = 350$ μm, presents the optimum value for this balance.

It is of particular interest to exploit the transition between lattice solitons and lattice filaments. Figure 3 shows simulations of Eq. (1) when the input pulse keeps the same temporal profile as before and the input beam corresponds to a lattice soliton for cylindrical [Fig. 3(a)] or rectangular lattices [Fig. 3(b)]. When all effects in Eq. (1) are ignored except diffraction and the optical Kerr effect, pulsed cylindrical lattice solitons remain quasistationary over extremely long propagation distances. When group velocity dispersion (GVD) and higher-order nonlinearities (multiphoton ionization, plasma defocusing, optical shock) are also taken into account, as in the filamentation dynamics, the propagation distance of lattice solitons dramatically reduces [5 m in the example of Fig. 3(a)]. In general, as the maximum intensity of the input lattice soliton increases and its beam width decreases, high-order effects become more important, leading to faster reshaping of the lattice soliton into a standard filament. Without the presence

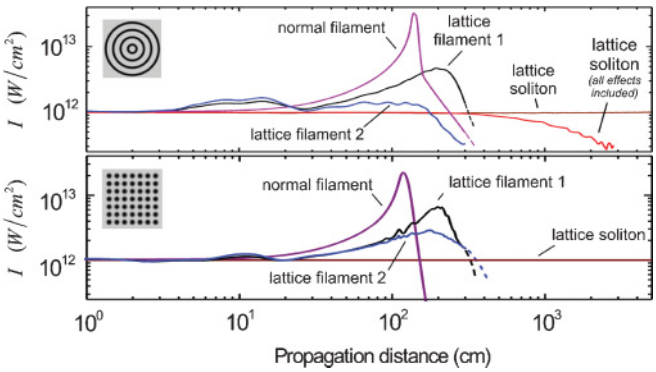

FIG. 3. (Color online) Peak intensity as a function of propagation distance, which reveals the transition dynamics between lattice solitons and lattice filaments. (a) The (2 + 1)-dimensional (cylindrically symmetric) simulations. (b) The (3 + 1)-dimensional (frozen time) simulations using a rectangular plasma lattice. Lattice soliton indicates the pulsed version of the cylindrical lattice soliton solution (taking into account only diffraction and Kerr effect). Lattice soliton (all effects included) indicates including GVD, multiphoton ionization, and plasma defocusing. Normal filament indicates typical filament in air from a Gaussian spatiotemporal pulse. Lattice filaments 1 and 2 indicate tailored lattice filaments for two different cases of lattice strength Δn. Insets are graphical representations of the lattices used in each case, where black represents lower refractive index.

of the lattice, a pulsed lattice soliton is rapidly self-focused, and a filament is formed, reaching intensities as high as 3×10^{13} W/cm^2 [normal filament in Fig. 3(a)]. The lattice regulates the pulse propagation, as is clearly shown in Fig. 3(a). The propagation distance of the lattice filaments and that of the lattice soliton (with all effects included) are in the same order of magnitude. More generally, our simulations show that the features of lattice filaments closely follow those of lattice solitons. Furthermore, filamentation tailoring by means of lattices is feasible with various types of lattices beyond the cylindrical lattices discussed here. For instance, results using rectangular lattices, obtained from $(3 + 1)$-dimensional simulations with "frozen" time (pulse duration fixed), are shown in Fig. 3(b) and demonstrate tailoring properties of filaments in a way similar to the cylindrical ones.

Finally, it is worth noting that the same approach of filamentation tailoring using lattices in gases can also be used for filaments in transparent solids. In that case the lattice can be either transient (like plasma lattices) or permanently written in the bulk in the form of an array of waveguides, which can be easily fabricated (see, for instance, [27]). Related results will be presented elsewhere.

In conclusion, we have presented a robust way to tailor the attributes of intense femtosecond laser filaments in transparent media by using lattices. By tuning the parameters of the lattice, we enforce the formation of a new kind of filament that can also be described as intense lattice solitons, with regulated attributes, such as their peak intensity, plasma density, beam waist, length, and uniformity. We have shown that this filamentation tailoring is not a linear guiding effect but a result of the balance between the nonlinear propagation effects and the linear diffraction induced by the lattice. In contrast to typical filaments, where self-action effects dominate and prohibit control over the filamentation attributes, we manage to gain control by introducing a lattice and appropriately tuning its period and modulation depth. Our approach opens the way for extensive control of the filament attributes in the spatial and temporal domains, with potentially a big impact on various applications utilizing filaments, such as tetrahertz generation or attosecond pulse generation, among many others.

This work was supported by the European Union Marie Curie Excellence Grant "MULTIRAD" MEXT-CT-2006–042683.

[1] A. Couairon and A. Mysyrowicz, Phys. Rep. **441**, 47 (2007).
[2] H. S. Chakraborty, M. B. Gaarde, and A. Couairon, Opt. Lett. **31**, 3662 (2006).
[3] A. Couairon *et al.*, Opt. Lett. **30**, 2657 (2005).
[4] S. Tzortzakis *et al.*, Phys. Rev. E **64**, 057401 (2001).
[5] J. Kasparian *et al.*, Science **301**, 61 (2003).
[6] X. Xie, J. M. Dai, and X. C. Zhang, Phys. Rev. Lett. **96**, 075005 (2006).
[7] K. Y. Kim *et al.*, Nat. Photonics **2**, 605 (2008).
[8] J. M. Manceau *et al.*, Opt. Lett. **34**, 2165 (2009); **35**, 2424 (2010).
[9] G. Fibich *et al.*, Opt. Lett. **29**, 1772 (2004).
[10] G. Mechain *et al.*, Phys. Rev. Lett. **93**, 035003 (2004).
[11] F. Calegari *et al.*, Phys. Rev. Lett. **100**, 123006 (2008).
[12] P. L. Kelley, Phys. Rev. Lett. **15**, 1005 (1965).
[13] M. I. Weinstein, Commun. Pure Appl. Math. **39**, 51 (1986).
[14] D. N. Christodoulides and R. I. Joseph, Opt. Lett. **13**, 794 (1988).
[15] H. S. Eisenberg *et al.*, Phys. Rev. Lett. **81**, 3383 (1998).
[16] V. K. Mezentsev *et al.*, JETP Lett. **60**, 829 (1994).
[17] S. Flach, K. Kladko, and R. S. MacKay, Phys. Rev. Lett. **78**, 1207 (1997).
[18] N. K. Efremidis *et al.*, Phys. Rev. Lett. **91**, 213906 (2003).
[19] J. K. Yang and Z. H. Musslimani, Opt. Lett. **28**, 2094 (2003).
[20] J. W. Fleischer *et al.*, Nature (London) **422**, 147 (2003).
[21] N. K. Efremidis *et al.*, Phys. Rev. E **66**, 046602 (2002).
[22] F. Lederer *et al.*, Phys. Rep. **463**, 1 (2008).
[23] S. Suntsov *et al.*, Appl. Phys. Lett. **94**, 251104 (2009).
[24] X. Yang *et al.*, Opt. Lett. **34**, 3806 (2009).
[25] M. Leibscher *et al.*, Phys. Rev. Lett. **90**, 213001 (2003).
[26] See supplementary material at [http://link.aps.org/supplemental/10.1103/PhysRevA.82.061803] for a detailed explanation of the numerical model used in the simulations.
[27] A. Szameit *et al.*, Opt. Express **14**, 6055 (2006).